Acta Neuropathologica Communications

RESEARCH

Open Access

Spatial transcriptomics in focal cortical dysplasia type IIb

Yujiao Wang[1,2,4,5†], Yihe Wang[3,4,5†], Linai Guo[1,4,5†], Chunhao Shen[3,4,5], Yongjuan Fu[1,4,5], Penghu Wei[3,4,5], Yongzhi Shan[3,4,5], Qian Wu[6], Yue-Shan Piao[1,4,5*] and Guoguang Zhao[3,4,5*]

Abstract

Focal cortical dysplasia (FCD) type IIb (FCD IIb) is an epileptogenic malformation of the neocortex that is characterized by cortical dyslamination, dysmorphic neurons (DNs) and balloon cells (BCs). Approximately 30–60% of lesions are associated with brain somatic mutations in the mTOR pathway. Herein, we investigated the transcriptional changes around the DNs and BCs regions in freshly frozen brain samples from three patients with FCD IIb by using spatial transcriptomics. We demonstrated that the DNs region in a gene enrichment network enriched for the mTOR signalling pathway, autophagy and the ubiquitin–proteasome system, additionally which are involved in regulating membrane potential, may contribute to epileptic discharge. Moreover, differential expression analysis further demonstrated stronger expression of components of the inflammatory response and complement activation in the BCs region. And the DNs and BCs regions exhibited common functional modules, including regulation of cell morphogenesis and developmental growth. Furthermore, the expression of representative proteins in the functional enrichment module mentioned above was increased in the lesions of FCD IIb, such as p62 in DNs and BCs, UCHL1 in DNs, and C3 and CLU in BCs, which was confirmed via immunohistochemistry. Collectively, we constructed a spatial map showing the potential effects and functions of the DNs and BCs regions at the transcriptomic level and generated publicly available data on human FCD IIb to facilitate future research on human epileptogenesis.

Keywords Focal cortical dysplasia type II, Spatial transcriptomics, Regulation of membrane potential, Complement activation, Inflammatory response, Drug-resistant epilepsy

†Yujiao Wang, Yihe Wang and Linai Guo contributed equally to this work.

*Correspondence:
Yue-Shan Piao
yueshanpiao@126.com
Guoguang Zhao
ggzhao@vip.sina.com
[1]Department of Pathology, Xuanwu Hospital, Capital Medical University, Beijing Municipal Geriatric Medical Research Center, Beijing 100053, China
[2]Department of Pathology, Shanxi Provincial People's Hospital, The Fifth Clinical Medical College of Shanxi Medical University, Taiyuan 030012, China
[3]Department of Neurosurgery, Xuanwu Hospital, Capital Medical University, Beijing 100053, China
[4]Clinical Research Center for Epilepsy, Capital Medical University, Beijing 100053, China
[5]National Center for Neurological Disorders, Beijing 100053, China
[6]State Key Laboratory of Cognitive Neuroscience and Learning, Beijing Normal University, Beijing 100875, China

Background

Focal cortical dysplasia (FCD) represents the most common cause of drug-resistant focal epilepsy in children and young adults [6, 8, 34]. Based on clinicopathological features, FCD can be classified into type 1 (FCD I), type 2 (FCD II) and type 3 (FCD III). The focal nature of FCD is histopathologically characterized by architectural and cytoarchitectural abnormalities, in which FCD type 2b (FCD IIb) lesions are distinguished from other FCDs by abnormal cells (that is dysmorphic neurons [DNs] and balloon cells [BCs]) [7, 8]. DNs cytoplasm significantly enlarged with accumulation of nonphosphorylated neurofilament isoforms (SMI-32), which is generally recognized as a marker for DNs. And BCs commonly accumulate intermediate filaments vimentin and nestin [9]. Most FCD I lesions show no visible magnetic resonance imaging (MRI) changes, due to the cellular density in the cortex being slightly altered with disorganization. MRI abnormalities in FCDII include abnormal gyration patterns indicated by a cortical dimple, cortical thickness changes, signal increase (mainly in FLAIR) both in the lesion and in the adjacent white matter, and blurring of the cortical-white matter junction. And the transmantle sign, a linear or triangular shaped high T2/FLAIR signal, indicates most likely FCDIIb [9, 34].

Recent studies have reported that 30–60% of lesions of FCD II harboured pathogenic variants in the mammalian target of rapamycin (mTOR) pathway-associated genes [4, 7, 17, 41]. Further molecular-genetic investigations are required to determine the underlying pathogenic cause in patients with FCD. In recent years, single-cell sequencing technology has been vigorously developed [21], including single-cell RNA-sequencing (scRNA-seq) and single-nucleus RNA-sequencing (snRNA-seq) technologies. The relatively large size and fragility of neurons largely restrict the application of scRNA-seq in the human brain. To date, single-cell expression profiles in the brain have mostly been generated by using snRNA-seq technology, especially for assessing neuronal genomics changes. On the other hand, isolated nuclear profiles from snRNA-seq have also limited our understanding of gene expression in the cytosol and neuropil. Thus, due to the larger size of DNs and BCs in comparison to neurons, we applied the Spatial transcriptomics (ST) [42] to explore the gene expression changes in FCD IIb.

Emerging ST technology has been applied to the research of Alzheimer's disease [11, 36], amyotrophic lateral sclerosis [29] and other neurological fields [22, 37, 48]; however, there is no research in the field of epilepsy, especially regarding FCD. Intact fresh frozen tissue sections are required for this technology to measure the whole spatial transcriptome. Visible MRI changes in FCD IIb further make it possible to obtain freshly resected tissues. A central question in FCD IIb research is the relationship of DNs and BCs to epileptogenesis. Herein, we used ST technology to identify genome-wide transcriptomic changes in FCD IIb focusing on DNs and BCs. Our results will lead to a novel insight to clarify the molecular mechanism of FCD.

Materials and methods

Human tissue

All of the patient protocols, which were authorized by the Ethics Committee of Xuanwu Hospital, Capital Medical University, conformed to the ethical principles of the Declaration of Helsinki, and written informed consent was acquired from all of the human subjects (number: [2021]068). Refractory epilepsy patients were examined at Xuanwu Hospital, Capital Medical University. Full epileptogenic evaluation was conducted on all of the patients, including electroencephalography (EEG), magnetic resonance imaging (MRI) and PET-CT. Patients were excluded from the study if there were metabolic abnormalities or any other systemic illness.

We collected four freshly frozen samples, the sequencing quality of which matched the criteria for further analysis, from three FCD IIb patients, all of whom originated from refractory epilepsy patients undergoing resection of epileptogenic lesions. Type II FCDs are more often easily visualized by MRI. Therefore, preoperative MRI-positive signs provide the first clue for FCD II. Afterwards, all of the patients were diagnosed with FCD IIb using intraoperative cryosection methods by two experienced neuropathologists.

Due to DNs can be distributed throughout the entire cortical layers. BCs can occur at any cortical region (including Layer 1) and are often found in the subcortical white matter. Therefore, we selected the grey-white-matter boundaries area with a high distribution of both DNs and BCs for lesional sampling and analysis. Four specimens were cut into small pieces of approximately $6.5\times6.5\times6.5$ mm^3. Then, frozen tissue blocks were post-embedded in prechilled Optimal Cutting Temperature (OCT, SAKURA, America). Cryosections were cut at 6 μm thickness. Haematoxylin-eosin staining (H&E) was used to confirm that three samples contained FCD IIb lesions, and one sample away from the lesion, which contained few cellular abnormalities and some hypertrophic neurons, was regarded as perilesion (Supplementary Fig. 1). Subsequently, the four samples analyzed by ST technology were embedded in paraffin and performed immunohistochemical staining. The immunostaining for pS6, SMI-32, and nestin further supports the morphological diagnosis, providing evidence for our selection of lesional and perilesional specimens (Supplementary Fig. 2).

RNA quality control

Cryosections were cut at 10 μm thickness onto ST slides by using a CryoStar NX70 cryostat (Thermo Fisher). We layered tissue sections onto a spatially barcoded array. Each spatially barcoded array has 4,992 gene expression spots, with a diameter of 55 mm and a centre-to-centre distance of 100 mm, over an area of 6.5 mm by 6.5 mm (10x genomics). RNA quality was checked by using RNeasy Mini Kit (QIAGEN, Hilden, Germany) and Agilent 2100 Bioanalyzer with RNA 6000 Pico Kit (Agilent Technologies, Inc., Santa Clara, CA, USA). The RNA integrity number (RIN) values of the tissues were between 7.29 and 8.22. Details of sample quality are described in Supplementary Table 2.

Histology staining and imaging for spatial transcriptomics

Fresh frozen sectioned tissues were mounted onto each capture area of the slide, wherein they were placed on a Thermocycler Adaptor with the active surface facing up, incubated for 1 min at 37 °C and fixed for 30 min with methyl alcohol at -20 °C. To perform H&E staining of the tissue, sections were incubated in Mayer's haematoxylin (Dako, S3309) for 7 min, after which Bluing buffer (CS702) was applied for 2 min, and eosin (Dako CS701) was applied for 20 s. The results were ultimately used to overlay gene expression patterns onto the image.

Permeabilizing the tissue

Visum spatial gene expression was processed by using Visum spatial gene expression slide and Reagent Kit (10x Genomics, PN-1000184). Then, 70 μl of permeabilization enzyme was added to the side of each well, and the slide was sealed and placed in a thermocycler adaptor at 37 °C. After incubation, the permeabilization enzyme was removed, and the wells were washed with 100 μl of 0.1 X saline sodium citrate (SSC) buffer (Sigma).

Reverse transcription, spatial library preparation and sequencing

The poly-adenylated mRNA released from the overlying cells was captured by the primers on the spots. The permeabilized tissues were incubated with 75 μl of reverse transcription (RT) Master Mix at 53 °C for 45 min to obtain stable cDNA attached to the array. At the end of first-strand synthesis, sections were incubated for 5 min at room temperature with 75 μl 0.08 M KOH. Afterwards, 75 μl of Second Strand Mix was added to each well for second-strand synthesis. cDNA amplification was performed on an S1000TM Touch Thermal Cycler (Bio-Rad). According to the manufacturer's instructions, Visum spatial libraries were constructed by using a Visum spatial Library construction kit (10x Genomics, PN-1000184). Sequencing handles and indices were added to a PCR, and the finished libraries were sequenced on an Illumina Novaseq6000 sequencer with a sequencing depth of at least 100,000 reads per spot with a paired-end 150 bp (PE150) reading strategy (CapitalBio Technology, Beijing).

Reads alignment and seurat analysis

Reads alignment, filtering, barcode counting, and UMI counting were performed with the Spaceranger (10x Genomics) count module to generate a feature-barcode matrix by using the default and recommended parameters. STAR Algorithm v2.5.1b was used to align the sequencing reads to Genome Reference Consortium Human Build 38.98 (GRCh38.98). R version 3.6.0 and the package Seurat v3.2 were used for the downstream analyses. Spots with fewer than 1,000 transcripts and more than 20% mitochondrial transcripts were removed.

Hierarchical clustering and cluster annotation

Dimensionality reduction was performed by using Principal component analysis (PCA), and the first 30 principal components (PCs) were used to generate clusters via the K-means algorithm and graph-based algorithm. We used Uniform Manifold Approximation and Projection (UMAP) to visualize ST clusters in a reduced 2D space. The RunHarmony function was employed to correct batch effects arising from multiple datasets. And the resolution of clustering is 0.8. For merged data, all of the replicate samples across the four patients were merged with the "merge" Seurat function and renormalized with SCTransform (regressing replicate and number of genes per spot) prior to PCA and UMAP on the first 30 PCs. Moreover, to assess the cellular region composition and differences between the lesions and perilesion, we merged digital expression matrices from three specimens of cases, namely lesion-1, lesion-2 and lesion-3. To identify differentially expressed genes, pairwise comparisons of individual clusters against all of the other clusters were performed by using the FindAllMarkers function in the Seurat package (version 3.2). Then, spatial distribution maps of each sample were compared with the previous HE staining photos for the same sample to further confirm the classification of the clusters.

Gene functional enrichment analysis

All of the differentially expressed genes with an average logFC value above zero and an adjusted p value below 0.01 were used for gene functional enrichment analysis, including Gene Ontology (GO) enrichment (i.e., GO-Biological Process (GO-BP), GO-Cellular Component [GO-CC] and GO-Molecular Function [GO-MF]) and Kyoto Encyclopedia of Genes and Genomes (KEGG) pathway enrichment.

Gene set enrichment analysis

Gene Set Enrichment Analysis (GSEA) was applied to identify significantly different gene sets between the two groups with GSEA software (version 4.0.3). A false discovery rate (FDR) value of 25% was selected to determine whether the enriched functional gene set was appropriate.

Immunohistochemistry

The remaining frozen tissues were embedded in paraffin and continuously sectioned into 6 μm thick sections. Immunohistochemical staining was performed as previously described [46]. We used brain tissues from three epilepsy patients with mild malformations of cortical development (mMCD) as control (Supplementary Fig. 10, Table 7). The following primary antibodies were used: anti-neuronal nuclear antigen (NeuN; Chemicon, USA, monoclonal, 1:4,000), anti-glial fibrillary acidic protein (GFAP; OriGene, USA, monoclonal, clone UMAB129, 1:200), anti-nonphosphorylated neurofilament (SMI32; Covance, USA, monoclonal, 1:400), anti-Nestin (R&D Systems, USA, monoclonal, 1:200), anti-pS6 (Cell Signaling Technology, USA, polyclonal, 1:200), anti-p62 (Sigma-Aldrich, USA, polyclonal, 1:1,000), anti-UCHL1 (Cell Signaling Technology, USA, polyclonal, 1:800), anti-CLU (Abcam, Britain, polyclonal, 1:200), and anti-C3 (Abcam, Britain, monoclonal, 1:8,000).

Results

Spatial transcriptomics identifies multiple regional signatures in human FCD IIb

We profiled spatial gene expression in four freshly frozen samples from three patients of FCD IIb, including three typical FCD IIb lesional specimens and one perilesional specimen comprising a few cellular abnormalities and containing a relatively complete neocortical structure (Supplementary Figs. 1, 2, 3). The clinicopathological features of the patient cohort were summarized in Supplementary Table 1. And the RNA integrity numbers (RINs) of all samples were in the range of 7.29–8.13 (Supplementary Table 2). Subsequently, the frozen tissue samples were placed on Visium slides for generation of sequencing data with a total of 12,754 spots, detecting on a mean of 7,601 unique molecular identifiers (UMIs) and a mean of 3,292 genes per spot (Fig. 1B).

We combined data from all subjects and used the Seurat v3.2 [43] R libraries for downstream analyses. Data were clustered to classify the spots and to determine the specific region type. Hereafter, we identified 13 different clusters (Clusters 0–12; Fig. 1E). Preliminary manual annotations of marker genes (STAR Methods) allowed us to identify cell classes. Cell type markers showed reliable prediction of cell identity (*NEFL*, *NEFM* and *NEFH* for DNs; *VIM* for BCs; *SLC17A7* and *SATB2* for excitatory neurons; *GAD1*, *GAD2*, *SST*, *VIP*, *CALB2* and *PVALB* for inhibitory neurons; *GFAP*, *AQP4*, *SLC1A2*, *SLC1A3* and *IGFBP7* for astrocytes; *MBP*, *PLP1*, *MOG*, *MOBP* and *CLDN11* for oligodendrocytes; *CCL3*, *CCL4L2* and *CCL4* for microglia; and *CLDN5*, *VWF*, *A2M*, *APOLD1* and *SLC2A1* for endothelial cells and pericytes; Fig. 1C). We next matched our results with histopathology to further confirm the classification of the clusters. These annotated cell regions include: Excitatory neurons region (Clusters 4 and 12), Inhibitory neurons region (Clusters 9 and 10), DNs region (Cluster 0), BCs region (Cluster 3), Astrocytes region (Clusters 2, 5 and 7), Microglia region (Cluster 11), Oligodendrocytes region (Clusters 1 and 6), Endothelial cells and Pericytes region (Cluster 8) (Fig. 1E, Supplementary Fig. 4). Particularly, among them, Cluster 0 and Cluster 3 expressed several known DNs or BCs markers, relatively consistent with the DNs or BCs morphological characteristics and distributions in histology (Fig. 1D, Supplementary Fig. 5).

Identification of the DNs region

We highlighted the differentially expressed genes in the DNs region. In addition to the classic DNs markers, *NEFH*, *NEFL* and *NEFM*, several genes had higher expression in the DNs domain, such as *ENC1*, *NRGN*, *VSNL1*, *OLFM1*, *CCK*, *CHN1*, *UCHL1*, *CRYM*, *YWHAH*, *MDH1*, *SNAP25*, *TUBB2A*, *NSF*, *GABRD*, *GAP43*, *NPTX2*, and *BASP1* (Fig. 2A, Supplementary Fig. 6). To understand changes in gene expression, we performed differential expression analyses by comparing Cluster 0 with all other clusters. Based on the GO enrichment analysis (Fig. 2B, Supplementary Fig. 7A, and Supplementary Table 3), we identified 6 major functional modules, including Synapse, Potential, Cell morphogenesis and developmental growth, Ubiquitination, Autophagy, and Microtubule. Among them, the most enriched functional classes of the DNs region were the regulation of membrane potential (GO:0042391; i.e., *YWHAH*, *SNAP25*, *NSF* and *GABRD*), synapse organization (GO:0050808; i.e., *NEFL*, *NEFH* and *GAP43*), proteasome-mediated ubiquitin-dependent protein catabolic process (GO:0043161; *UCHL1*), regulation of cellular component size (GO:0032535; i.e., *NEFL*, *NEFH*, *ENC1*, *OLFM1*, *CCK*, *CHN1*, *YWHAH*, *GAP43* and *BASP1*), macroautophagy (GO:0016236; i.e., *ENC1*), and regulation of microtubule-based process (GO:0032886; i.e., *NEFL*, *NEFM*, *NEFH* and *TUBB2A*). We performed Z-scored mean log expression heatmap on genes related to the regulation of membrane potential and proteasome-mediated ubiquitin-dependent protein catabolic process, further confirming that these genes are mainly expressed in the DNs region (Fig. 2E, F). In addition, we found that the DNs region was involved in Proteasome (hsa03050), Ubiquitin mediated proteolysis (hsa04120), Phosphatidylinositol signalling system

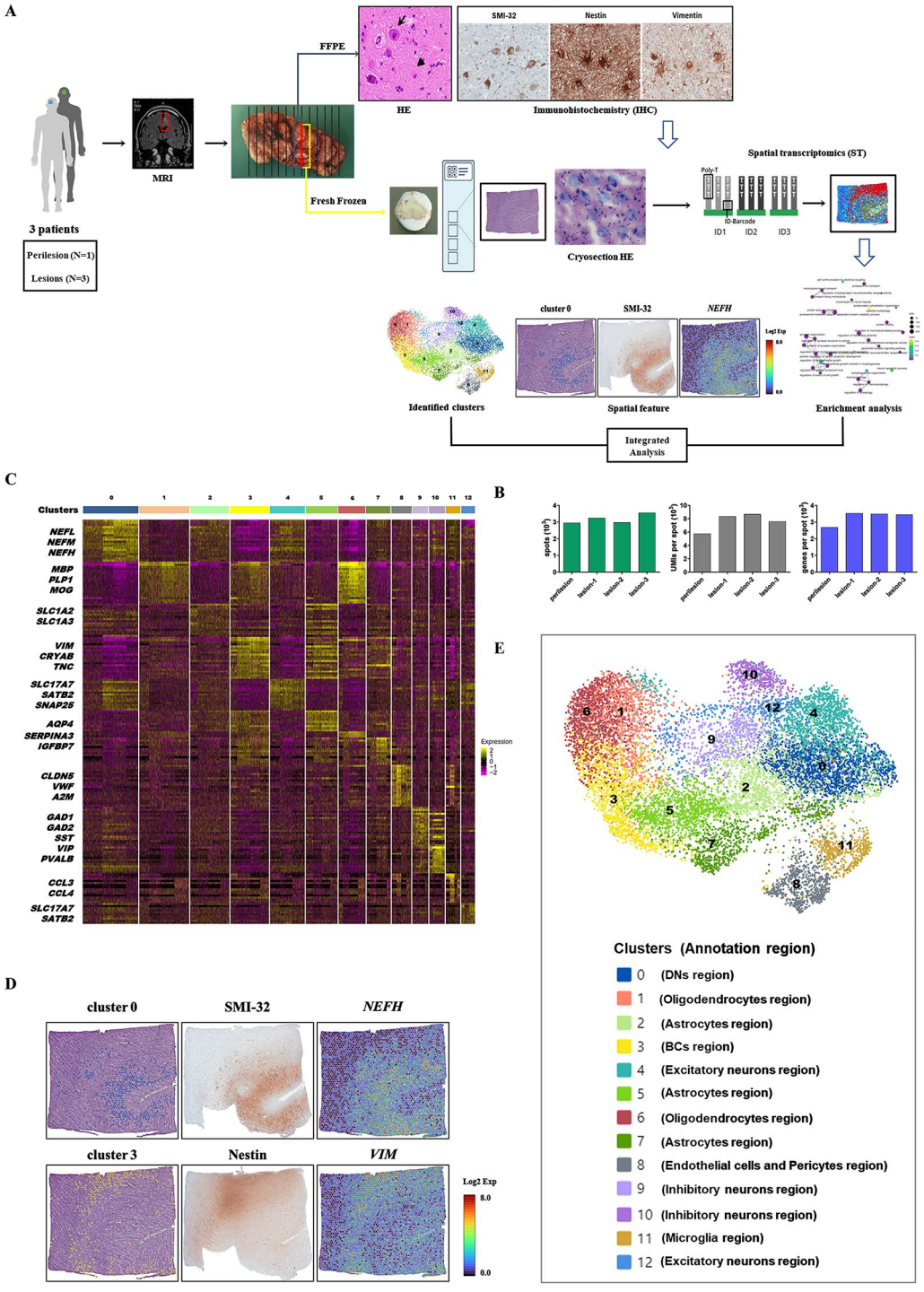

Fig. 1 ST analysis of four samples from three patients with FCD IIb. **(A)** Workflow of FCD IIb patient sample processing for ST. Four freshly frozen samples from three FCD IIb patients were collected. First, preoperative MRI positive signs provide the first clue for FCD II. Second, macroscopic abnormal tissues (yellow) were freshly frozen for intraoperative cryosection diagnosis by two experienced neuropathologists, thus confirming that three samples contained FCD IIb lesions, and few cellular abnormalities were present in one perilesion. Then, its' mirror plane tissues (blue) were prepared for formalin-fixed paraffin embedding (FFPE) and immunostaining. Finally, the qualified samples were applied the ST technology to explore the gene expression changes in FCD IIb. **(B)** Number of Visium spots (left), UMIs per spot (middle), and genes per spot captured (right) are shown per subject. **(C)** Heatmap showing representative marker genes for each cluster. **(D)** From left to right: the Spatial feature plots of Cluster 0 (top) and Cluster 3 (bottom), immunohistochemistry of SMI-32 (top) and Nestin (bottom), and ST feature plots of NEFH (DNs marker, top) and VIM (BCs marker, bottom) expression in lesion-1. **(E)** Thirteen regions (Clusters 0–12) were identified and visualized by using UMAP

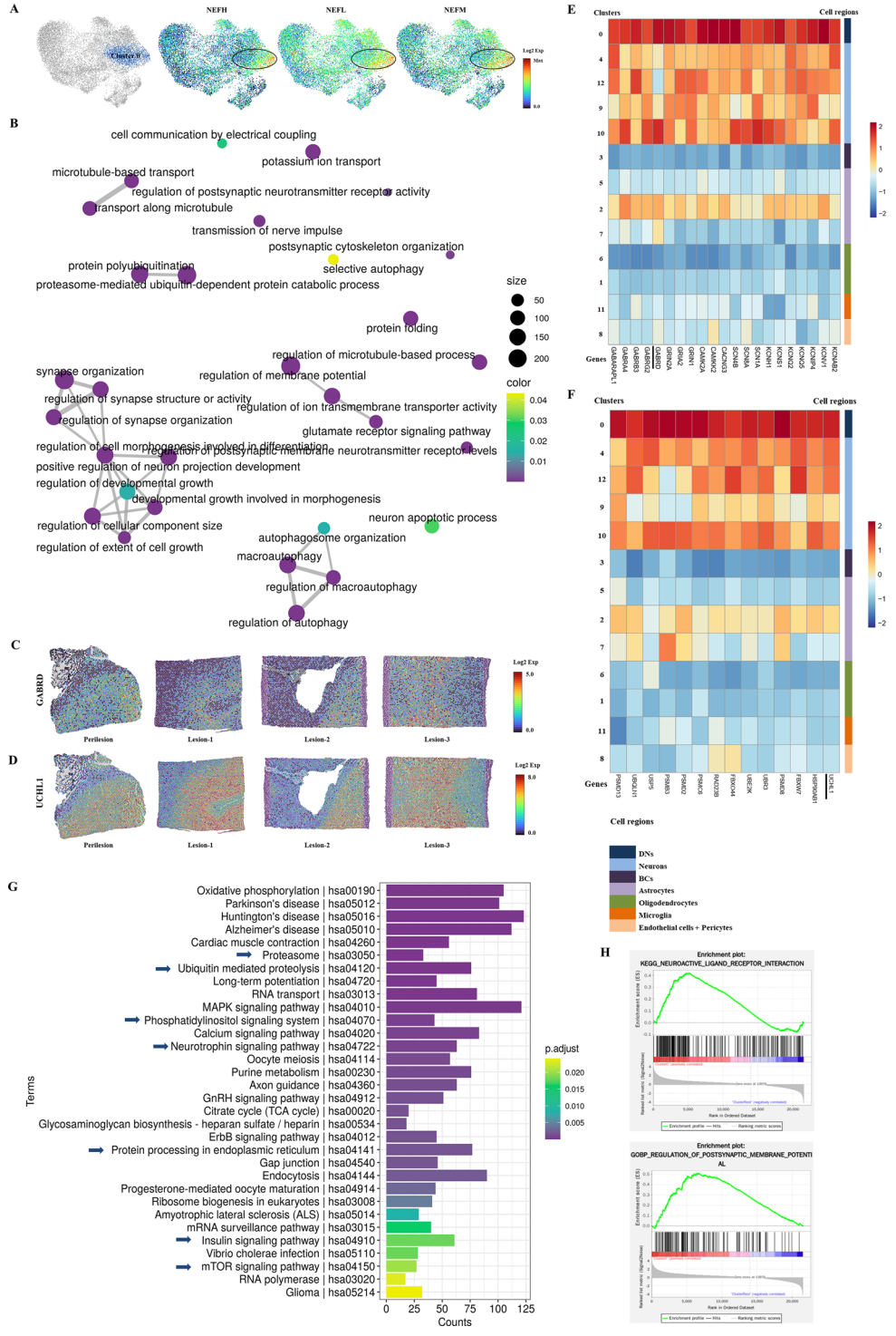

Fig. 2 Identification of the DNs region. **(A)** Left, the DNs region (Cluster 0) was identified and visualized by using UMAP. Right, UMAP feature plots of expression for the DNs-specific genes *NEFH*, *NEFL*, and *NEFM*. **(B)** Enrichment map of GO-BP terms for Cluster 0. **(C)**, **(D)** ST feature plots of representative genes *GABRD* and *UCHL1* expression in four samples. **(E)**, **(F)** Z-scored mean log expression heatmap of genes associated with the regulation of membrane potential, and proteasome-mediated ubiquitin-dependent protein catabolic process across the annotated cell regions in the ST data. **(G)** Bar plots of KEGG terms for Cluster 0. **(H)** GO-BP and KEGG analyses on the DNs region (Cluster 0 vs. Cluster rest) applied by GSEA enrichment

(hsa04070), Neurotrophin signalling pathway (hsa04722), Protein processing in endoplasmic reticulum (hsa04141), Insulin signalling pathway (hsa04910), and mTOR signalling pathway (hsa04150) by using KEGG functional enrichment analysis (Fig. 2G). And the Gene-Concept Networks by KEGG analysis exhibited complex interactions between several pathways (Supplementary Fig. 7B).

To further investigate the gene functions in the DNs region, we performed gene set enrichment analysis (GSEA). These collections of gene sets allowed us to analyse the activity of groups of biologically related genes. We applied GSEA to identify the DNs region (Cluster 0) compared with the other cellular regions (without Cluster 0). All of these sets were clearly related to Cluster 0 functions. The sets were (i) an annotated collection of genes involving the regulation of postsynaptic membrane potential (GO-BP) (Fig. 2H); (ii) a biologically annotated collection of genes involved in neuroactive ligand receptor interaction (KEGG) (Fig. 2H); (iii) an annotated collection of genes association with synaptic membrane (e.g., postsynaptic membrane, presynaptic membrane, GABA ergic synapse, and glutamatergic synapse), and ion channel complex (e.g., GABA receptor complex, potassium channel complex, voltage-gated calcium channel complex, and voltage-gated sodium channel complex) (GO-CC) (Supplementary Table 4); and (iv) an annotated collection of genes enriched in ion channel activity (e.g., voltage-gated cation channel activity, extracellular ligand-gated ion channel activity, GABA receptor activity, potassium channel activity, voltage-gated cation potassium channel activity, voltage-gated sodium channel activity, and voltage-gated calcium channel activity [GO-MF]) (Supplementary Table 4). We also applied GSEA to identify the DNs region (Cluster 0) compared with Neurons region (Clusters 4, 9, 10 and 12), Excitatory neurons region (Clusters 4 and 12), and inhibitory neurons region (Clusters 9 and 10), without an appropriate enriched functional gene set to meet the filter criteria.

Taken together, these data yielded unanimous results that the DNs region in FCD IIb is mainly associated with the mTOR signalling pathway, autophagy, and the ubiquitin-proteasome system, which might be the underlying mechanism contributing to the occurrence of abnormal cell morphology in FCD. Moreover, the results suggested that the DNs region may be involved in epileptic discharge via regulating membrane potential.

Identification of the BCs region

We analysed the top 20 genes that were significantly elevated in the BCs region (*VIM*, *CRYAB*, *EFEMP1*, *TNC*, *CLU*, *IGFBP7*, *SPARC*, *GPNMB*, *PTGDS*, *MAOB*, *MGST1*, *APOE*, *ANXA1*, *SERPINA3*, *AEBP1*, *GSN*, *GJA1*, *C3*, *CSRP1*, and *AQP4*) (Fig. 3A, Supplementary Fig. 8). Afterwards, we performed differential expression analyses by comparing Cluster 3 with all other clusters. Based on the GO enrichment analysis, we identified 6 major functional modules, including Actin filament, Cell morphogenesis and developmental growth, Neural precursor cell proliferation, Reactive oxygen metabolize, Complement activation, and Inflammatory response (Fig. 3B, Supplementary Table 5). We further demonstrated in detail that Cluster 3 is involved in actin filament organization (GO:0007015; i.e., *VIM*, *CRYAB* and *GSN*), glial cell differentiation (GO:0010001; i.e., *VIM*, *CLU* and *GSN*), reactive oxygen species metabolic process (GO:0072593; i.e., *CRYAB*, *APOE* and *ANXA1*), and developmental growth involved in morphogenesis (GO:0060560; i.e., *CLU*, *IGFBP7*, *APOE*, *ANXA1*, *GSN*, and *GJA1*). Moreover, we observed that the BCs region not only has strong associations with complement activation (GO:0006956; i.e., *CLU* and *C3*), regulation of complement activation (GO:0030449; i.e., *CLU* and *C3*), but also with effector mechanisms triggered by the complement cascade, such as phagocytosis (GO:0006909; i.e., *C3*, *ANXA1* and *GSN*), and immune response (i.e., *C3*, *CLU*, and *SERPINA3*), including acute inflammatory response (GO:0002526), regulation of acute inflammatory response (GO:0002673), and regulation of humoral immune response (GO:0002920). Moreover, we next analysed the expression of genes related to complement activation, mostly focused on the BCs region (Fig. 3E). In addition, most of the differentially expressed genes in the BCs region were significantly enriched in Phagosome (hsa04145), Regulation of actin cytoskeleton (hsa04810), Focal adhesion (has04510), Antigen processing and presentation (hsa04612) and Allograft rejection (hsa05330) (Fig. 3C, D). Collectively, these data indicated that the inflammatory response and complement activation may play a role in the pathogenesis of BCs region.

Identification of the lesion and perilesion in human FCD IIb

Afterwards, we investigated the differences between lesions and perilesion in human FCD IIb (Fig. 4A). The top 20 differentially expressed genes were significantly elevated in the lesions (Fig. 4B, Supplementary Fig. 9). Of note, the levels of *SERPINA3*, which is a marker of reactive astrocytes, were significantly elevated in lesions compared with perilesional tissue of FCD IIb. *SPARC* and *CHI3L1* were both related to blood vessel development, and *CHI3L1* expression was reported in a unique population of small cells in close proximity to BCs, most likely to be glial progenitors [26]. As a whole, genes involved in nervous system development included *GFAP*, *PLP1*, *SPP1*, *VIM*, *CLDN11*, *CLU*, *S100B*, *SELENOP* and *CNP*. We also identified 7 genes enriched in cell morphogenesis, such as *SPARC*, *SPP1*, *IGFBP7*, *FAM107A*, *S100B*, *GPNMB*, and *CNP*. Some molecules, such as *SERPINA3*, *SPARC*, *CHI3L1*, *PLP1*, *SPP1*, *CD74*, *CRYAB*, *TAC1*,

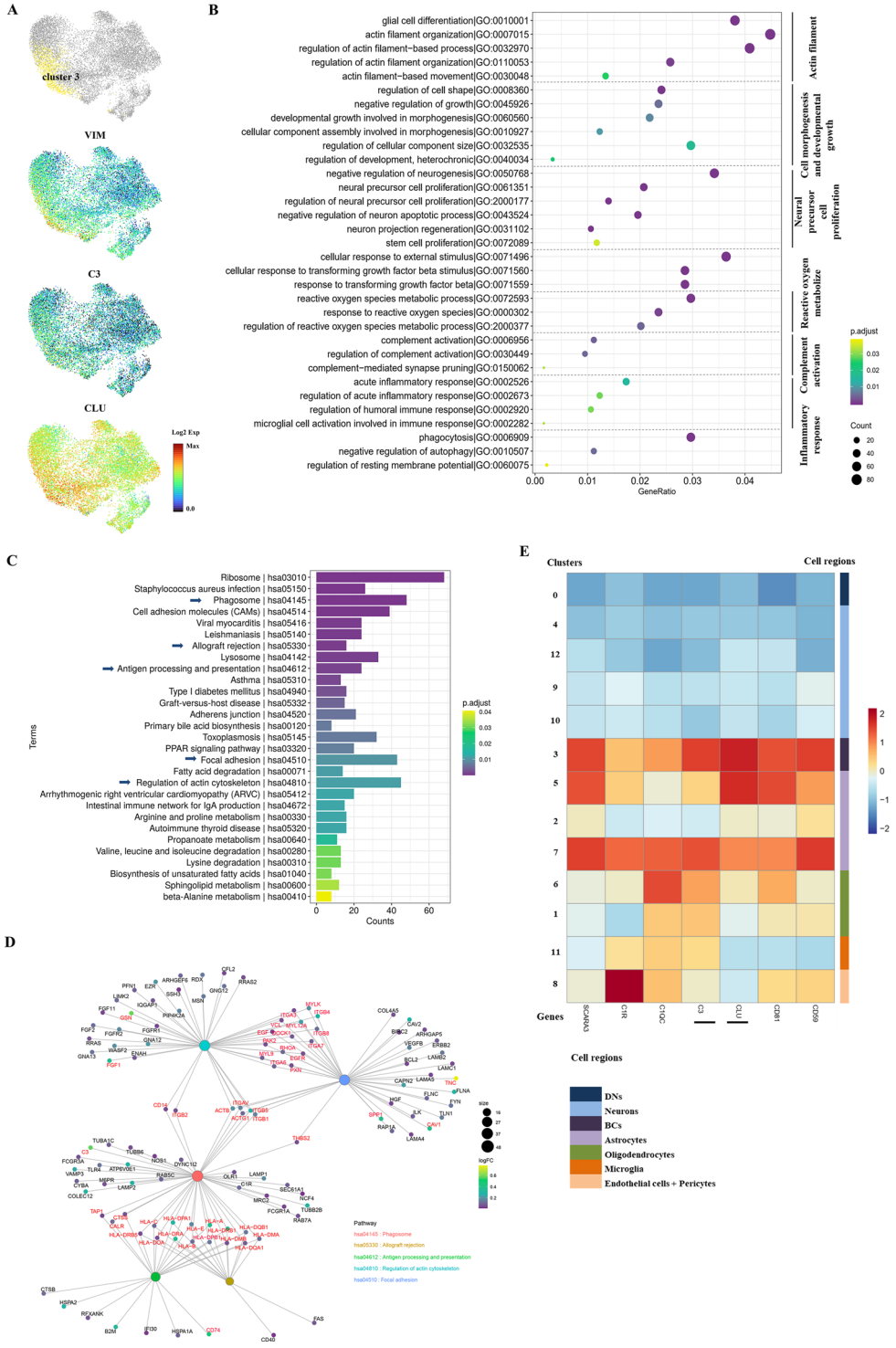

Fig. 3 Identification of the BCs region. **(A)** Left, the BCs region (Cluster 3) was identified and visualized by using UMAP. Right, UMAP feature plots of expression for BCs-specific genes *VIM*, *C3* and *CLU*. **(B)** Dot plot of GO-BP terms for Cluster 3. **(C)**, **(D)** Bar plots and Gene-Term Network of KEGG terms for Cluster 3. **(E)** Z-scored mean log expression heatmap of genes associated with complement activation across the annotated cell regions in ST data

CLU, *C3*, *S100B*, and *GPNMB*, showed reliable associations with the inflammatory response. In addition, genes such as *CLU* and *C3* were involved in complement activation (Supplementary Table 6).

We subsequently analysed the functional differences of the DNs or BCs region between the lesions and perilesion in more detail. Based on the GO enrichment analysis (Fig. 4C, D), the DNs and BCs regions exhibited shared

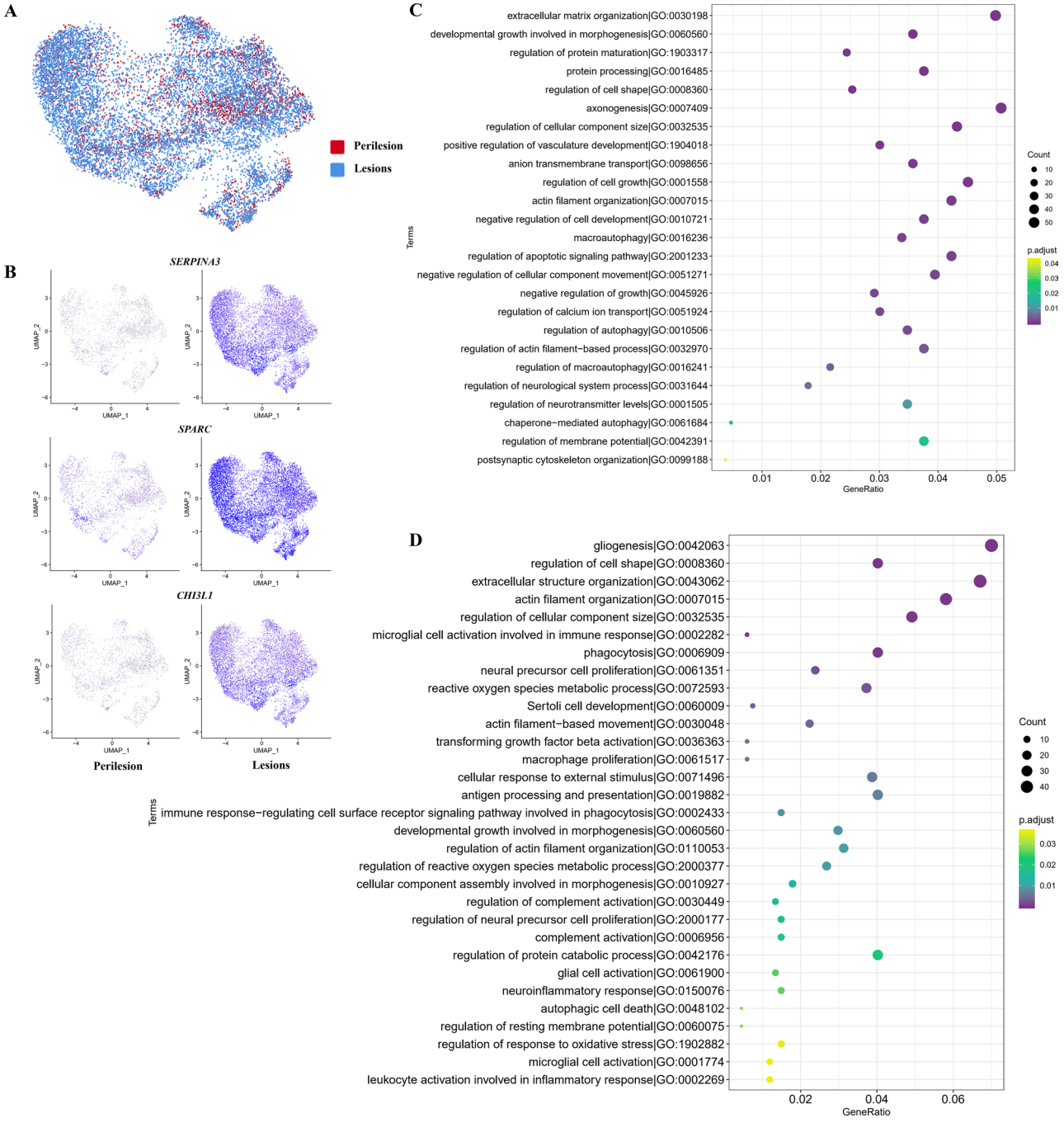

Fig. 4 Differences in the lesions and perilesion in human FCD IIb. **(A)** The regions of perilesion and lesions were identified and visualized by using UMAP. **(B)** UMAP plots of representative *SERPINA3*, *SPARC* and *CHI3L1* gene expression in perilesion and lesions. **(C)** Dot plot of GO-BP terms for Cluster 0 (DNs region) between the lesions and perilesion. **(D)** Dot plot of GO-BP terms for Cluster 3 (BCs region) between the lesions and perilesion

functional modules, regulation of cell morphogenesis and developmental growth (i.e., GO:0008360, regulation of cell shape; GO:0032535, regulation of cellular component size; and GO:0060560, developmental growth involved in morphogenesis). Similarly, the differentially expressed genes in the DNs region were enriched in Autophagy (i.e., GO:0016236, macroautophagy; GO:0010506, regulation of autophagy; GO:0016241, regulation of macroautophagy; and GO:0061684, chaperone-mediated autophagy) and Potential (i.e., GO:0042391, regulation of membrane potential; and GO:0098656, anion transmembrane transport). Several functional modules were identified in the BCs region (Fig. 4D), including Inflammatory response (i.e., GO:0150076, neuroinflammatory response; GO:0002269, leukocyte activation involved in inflammatory response; and GO:0002282, microglial cell activation

involved in immune response, etc.), Complement activation (i.e., GO:0006956, complement activation; and GO:0030449, regulation of complement activation), Reactive oxygen metabolize (i.e., GO:0072593, reactive oxygen species; and GO:2000377, regulation of reactive oxygen species metabolic process), and Neural precursor cell proliferation (i.e., GO:0061351, neural precursor cell proliferation; and GO:2000177, regulation of neural precursor cell proliferation).

Immunohistochemistry provides protein visualization of the DNs and BCs regions

To understand gene functional enrichment in the DNs and BCs regions of FCD IIb, we performed immunohistochemical staining for representative genes that encoded for proteins in the mTOR signalling pathway, autophagy, the ubiquitin-proteasome system, inflammatory response and complement activation.

Activation of the mTOR pathway has been linked to the cytopathology of FCD. As expected, genes involved in the mTOR signalling pathway, such as *PIK3R3*, *AKT3* and *RHEB*, were mainly enriched in the DNs region. We also detected phosphorylated ribosomal S6 protein (pS6) expression via immunohistochemistry (IHC). DNs showed a striking cytoplasmic labelling pattern with the pS6 marker, whereas BCs also showed pS6 immunopositivity but were less intensely labelled than the DNs, thus providing evidence for mTOR pathway activation in FCD IIb.

Autophagy dysregulation is partially dependent on mTOR pathway activation. Genes associated with autophagy were mostly expressed in the neuronal regions, not specific to the DNs region in the transcriptome level. Then, we examined the expression of p62, the critical component of the autophagy pathway, in FCD. Prominent cytoplasmic accumulation of p62 protein in the DNs and a proportion of BCs indicated an abnormality of autophagy in FCD II b (Fig. 5B).

The ubiquitin proteasome system (UPS), which is essential for removing abnormal proteins, cooperates with autophagy to maintain macromolecular homeostasis. Genes involved in the UPS that were mostly specific to the DNs region, such as *UCHL1*, *HSP90AB1*, *FBXW7*, *PSMD8*, *UBR3*, *UBE2K*, *FBXO44*, *RAD23B*, *PSMC6*, *PSMD2*, *PSMB3*, *USP5*, *UBQLN1*, and *PSMD13* (Fig. 2F). UCHL1 is a multifunctional protein expressed in neurons in the brain [30]. We found that UCHL1 is mainly expressed in neurons of mMCD (Supplementary Fig. 10), but significantly aggregates in the cytoplasm of DNs (Fig. 5B), thus suggesting dysregulation of the UPS in FCD IIb, which may contribute to the occurrence of abnormal cell morphology.

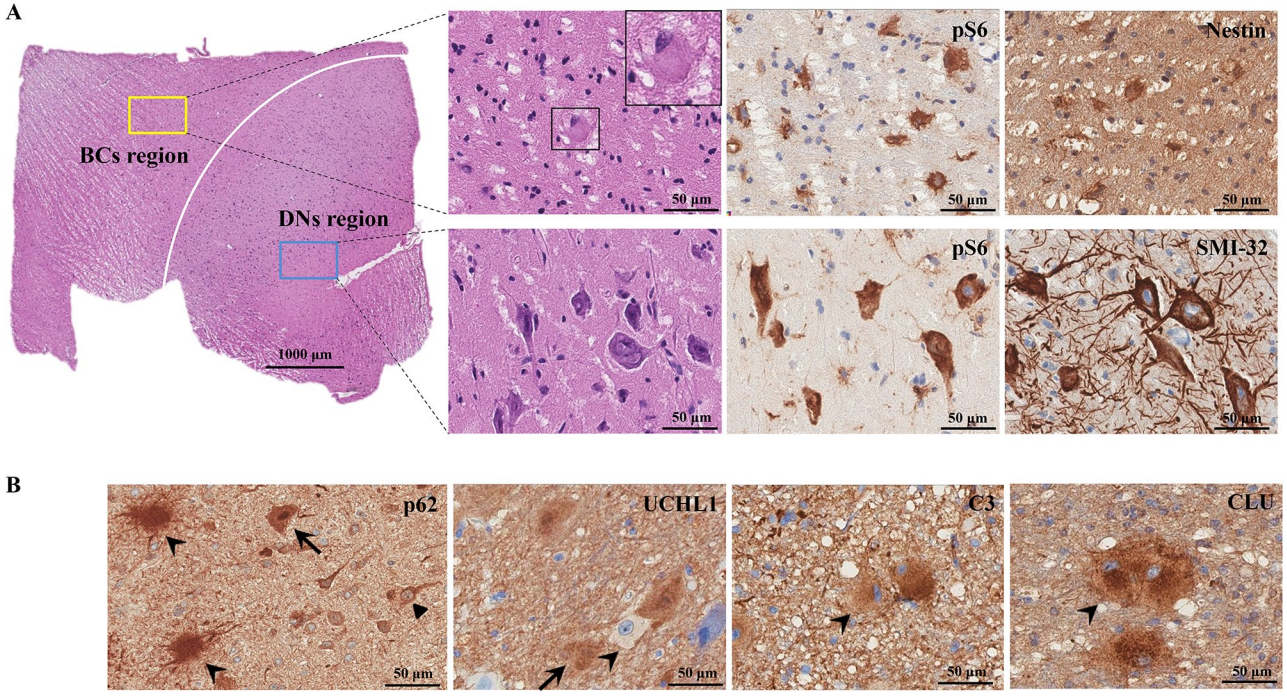

Fig. 5 Immunohistochemical staining for representative proteins in FCD IIb. **(A)** Left, macroscopic HE image of a case (lesion-1) with identification of the DNs region and BCs region. The white line represents the virtual border between the cortical and white matter regions. Right, microscopically, dysmorphic neurons (DNs) and balloon cells (BCs) and relevant markers, including positive pS6 immunostaining for both, positive Nestin immunoreactivity for BCs, and strong SMI-32 immunoreactivity for DNs. **(B)** Positive p62 immunostaining in the DNs (arrow), BCs (arrowhead) and neurons (triangle) were observed. UCHL1 staining confirming cytoplasmic labelling in the DNs. However, frequent cytoplasmic labelling of C3 and CLU proteins were observed in the BCs

Additionally, to identify whether the products of the inflammatory response and complement activation are deposited in the BCs region, we performed immunohistochemical staining for complement C3 (C3) and the complement cascade inhibitor clusterin (CLU). C3 and CLU were expressed in astrocytes of mMCD (Supplementary Fig. 10), but showing a striking cytoplasmic labelling pattern in the BCs (Fig. 5B), indicating existence of inflammatory and anti-inflammatory factors co-regulates the immune inflammatory network in the brain tissues of FCD IIb.

Discussion

Spatial Transcriptomics has provided a new paradigm for understanding FCD. We generated a large dataset of transcriptional changes in the human FCD IIb brain tissues by ST technology. Herein, we focused on the transcriptomic changes in cytoarchitectural abnormalities of FCD, including the DNs and BCs regions. To be precise, the DNs region (Cluster 0) and BCs region (Cluster 3) represent the intercellular microenvironment of a specific region that mainly contains the DNs and BCs. The data bring together several pathways that have been implicated separately in FCD IIb. We found that the DNs region in FCD IIb was mainly associated with the mTOR signalling pathway, autophagy, and the ubiquitin-proteasome system, particularly may be involved in epileptic discharge via regulating membrane potential. Moreover, we also identified that the inflammatory response and complement activation may play a role in the BCs region.

Intrinsic epileptogenicity has been reported in FCDs. Several studies have attempted to define electrophysiological abnormalities in FCD, indicating that the primary driving force for these pathological discharges is GABAergic rather than glutamatergic transmission [5, 10]. Our previous research has indicated that altered GABAergic inhibitory action, partially attributed to imbalanced function of NKCC1/KCC2 by affecting chloride ion homeostasis in neurons, contributes to epileptogenesis in FCDs [28]. Furthermore, GABA receptor signalling persistence in the immature CNS may conduce to hyperexcitability within FCD IIb, especially $GABA_A$ receptors [5, 16, 53], and spontaneous postsynaptic currents are displayed by neurons rather than BCs and intermediate cells [10]. Our study found that $GABA_A$ gated chloride ion channel activity-related genes, including *GABRD* (gamma aminobutyric acid type A receptor subunit delta), *GABRB3* (gamma aminobutyric acid type A receptor subunit beta3), *GABRA4* (gamma aminobutyric acid type A receptor subunit alpha4) and *GABARAPL1* (GABAA type A receptor associated protein like 1), were mainly expressed in the DNs region (Fig. 2E). In addition, we observed that the gene *GABRD*, which is responsible for persistent tonic inhibition and is abundantly expressed at extrasynaptic locations in the hippocampus, amygdala, neocortex, thalamus, hypothalamus and cerebellum, here, was highly expressed in the DNs region. However, the function and mechanism of *GABRD* in FCD IIb are still unclear. An analysis of targeted gene sequencing in patients with neurodevelopmental disorders and epilepsy concluded that *GABRD* variants are unlikely to be associated with epilepsy [20]. In contrast, recent studies have indicated that the gain-of-function variants in *GABRD* (such as increased receptor activity) demonstrated a novel pathway that causes severe neurodevelopmental disorder and leads to generalized epilepsy [1]. Moreover, *YWHAH*, *SNAP25* and *NSF* were also highly expressed at the DNs region and closely related to the function of regulating membrane potential. YWHAG regulates the Na+current to affect cell membrane potential, and its variants have been reported to cause developmental and epileptic encephalopathy or autism [50]. SNAP25 is a member of the SNARE complex for neurotransmitter release. Recent studies have reported that SNAP25 mutations give rise to developmental and epileptic encephalopathies [2]. NSF may affect spontaneous network excitation in epilepsy by controlling transmitter release at the presynaptic side or directing specific receptor compounds into the postsynaptic membrane [19]. Our results further indicated that DNs may generate or sustain epileptiform activity via regulating membrane potential at the transcriptome level.

Growing evidence suggests that brain somatic gene mutations are frequently detected in type II FCD foci, and most genes belong to the mTOR pathway (*PTEN*, *PIK3CA*, *TSC1*/*TSC2*, *NPRL2*, *NPRL3* and *DEPDC5*) [4, 17, 27, 41], although the variant allelic fraction (VAF) is low (often < 5%). Additionally, our previous study identified frequent *MTOR* mutations in the cell-rich FCD IIb phenotype, which is clinically characterized by a non-temporal location and large lesion volume [47]. Brain somatic mosaicism can lead to aberrant activation of mTOR kinase, thus resulting in brain malformations. Therefore, this could serve as a crucial pathogenic mechanism leading to intractable epilepsy [25, 35, 44]. In our series, we found that several genes in the DNs region were involved in the mTOR signalling pathway via KEGG functional enrichment analysis. In addition, pS6, the robust biomarker for mTOR signalling pathway activation [15], showed remarkable immunoreactivity in both DNs and BCs, providing a clue for mTOR cascade activation in FCD IIb, which is consistent with the published literature [3, 15, 23]. Moreover, autophagy is impacted by mTOR, and the activation of the amino acid-responsive MTOR kinase complex is a key signal for autophagosome inhibition by phosphorylating Atg13 and ULKs [33]. Autophagy is a catabolic pathway that plays a housekeeping role in removing misfolded or aggregated proteins

and for clearing damaged organelles [31]. We identified one of the major functional modules based on the GO enrichment analysis, such as Autophagy on the DNs region, including autophagosome organization, macroautophagy, regulation of macroautophagy, and regulation of autophagy. Also, the accumulation of p62 protein in DNs and a proportion of BCs indicated an inhibition of autophagy in FCD IIb. Overall, we hypothesized that aberrant autophagy plays a key role in epilepsy by two mechanisms of action: (1) via accumulation of misfolded or aggregated proteins contributing to the occurrence of abnormal cell morphology in FCD, and (2) possibly via enhancing anomalous axon plasticity, synaptic remodelling and, ultimately, the formation of epileptic networks [14].

The other cellular quality control pathway is the ubiquitin-proteasome system (UPS), which specifically degrades ubiquitin-labelled proteins [38]. The UPS consists of ubiquitin (Ub), ubiquitin-activating enzyme (E1), ubiquitin-conjugating enzyme (E2), ubiquitin protein ligase (E3), the 26 S proteasome and deubiquitinating enzymes (DUBs). The genes related to the UPS in our series were enriched in the neuronal region and were especially expressed in the DNs region. Among them, UCHL1, which possesses both ubiquitin E3 ligase and hydrolase activities, was highly expressed in the DNs region. Dysregulation of the UCHL1 has been implicated in numerous diseases, including Alzheimer's disease (AD), Parkinson's disease (PD) and epilepsy [30, 39]. Inhibition of UCHL1 activity significantly increased concentrations of amyloid β, whereas overexpression of UCHL1 decreased amyloid β levels and delayed AD progression [51]. Moreover, s-nitrosylation of UCHL1 induces structural instability and promotes α-synuclein aggregation in Lewy bodies [24], demonstrating that UCHL1 plays critical roles in PD pathogenesis. A previous study noted that UCHL1 concentrations in CSF and plasma were significantly higher in patients with recurrent seizures than in those after one or two seizures and in controls [32]. This suggested that UCHL1 may become a biomarker of epileptogenesis. However, the function of UCHL1 in FCD IIb is still unclear and requires further research.

Recent studies have illustrated that inflammatory changes may facilitate epileptogenesis [13, 40, 45]. Wu et al. demonstrated that the upregulation of the HMGB1-TLR4 inflammatory pathway in FCD type II lesions, e.g., TLR4, IL-1β and TNF-α [52], thus indicating that inflammation may cause seizures in FCD. In our cohort, differential expression analysis further revealed intense expression of components of the inflammatory response (e.g., *SERPINA3*) and complement activation (e.g., *C3* and *CLU*) in the BCs region compared with the other regions, particularly in lesions compared with the perilesion of FCD IIb. Similar to previous studies, upregulation of markers involved in neuroinflammation was found in the BCs and the surrounding environment, such as *SERPINA3*, *SPARC*, and *CHI3L1* [26], etc. Our findings suggest that neuroinflammation may be an important mechanism that contributes to the pathogenesis and epileptogenesis of FCD lesions. In addition, Aronica et al. also indicated stronger upregulation of complement factors in FCD II b, such as early complement factors C1–C4; in particular, zones rich in malformed cells displayed stronger C1q and C3d reactivity than the surrounding region [54]. They concluded that BCs are crucial drivers of inflammation in FCD II b, and our data also showed similar results. In the brain, CLU is largely produced by astrocytes [12, 49] but is mainly expressed in the BCs in our results. As a complement inhibitor, CLU was reported to reduce brain inflammation by targeting the vasculature [18], although other mechanisms are probably also involved. Moreover, neurons cocultured with CLU-overexpressing astrocytes displayed enhanced excitatory neurotransmission [12]. Hence, the function of CLU in FCD IIb possibly involves reducing inflammation or promoting excitatory synaptic transmission or other mechanisms, which requires further research. Overall, our results suggested that the BCs region in FCD IIb displays prominent neuroinflammation and complement system activation.

In this study, we provide a spatial map of human FCD IIb by using the recent ST technology, which contributed to the understanding of the tissue distribution of the main abnormal cell populations (DNs and BCs) that characterize this epileptogenic lesion. Furthermore, our combined analyses suggest that the DNs region may be involved in epileptic discharge to cause epileptogenesis by regulating membrane potential, accompanied by dysregulation of the mTOR signalling pathway, autophagy, and the ubiquitin-proteasome system. These pathways may contribute to cellular proliferation, accumulation of misfolded or aggregated proteins, leading to the occurrence of abnormal cell morphology. Moreover, despite the variability, the BCs region may promote neuroinflammation and complement activation in FCD IIb lesions, further facilitate epileptogenesis. Due to the lack of single-cell RNA sequencing data and functional ex vivo data, different cell subtypes could not be accurately assorted, and some molecules or pathway effects in FCD IIb could not be verified, which remain to be explored deeply in detail.

Abbreviations

FCD	Focal Cortical Dysplasia
FCD IIb	Focal Cortical Dysplasia type 2b
ST	Spatial Transcriptomics
DNs	Dysmorphic Neurons
BCs	Balloon Cells
MRI	Magnetic Resonance Imaging
scRNA-seq	single-cell RNA-sequencing

snRNA-seq	single-nucleus RNA-sequencing
RINs	RNA integrity numbers
UMIs	Unique Molecular Identifiers
pS6	phosphorylated ribosomal S6 protein
IHC	Immunohistochemistry
UPS	Ubiquitin Proteasome System
UMAP	Uniform Manifold Approximation and Projection
PCA	Principal Component Analysis
GO	Gene Ontology
GO-BP	GO-Biological Process
GO-CC	GO-Cellular Component
GO-MF	GO-Molecular Function
KEGG	Kyoto Encyclopedia of Genes and Genomes
GSEA	Gene Set Enrichment Analysis
C3	Complement C3
mTOR	mammalian Target Of Rapamycin
VAF	Variant Allelic Fraction

Supplementary Information

The online version contains supplementary material available at https://doi.org/10.1186/s40478-024-01897-7.

Supplementary Material 1

Supplementary Material 2

Acknowledgements
We kindly thank Ze-liang Hu, Li-hong Zhao and Dr. Wen-qiang Che for their technical assistance.

Author contributions
Y.J.W. and Y.S.P. contributed to the conception and design of the study; Y.J.W., Y.H.W., P.H.W., Y.Z.S., L.A.G., C.H.S., Y.J.F., and Y.S.P. contributed to the acquisition and analysis of data; Y.J.W., Q.W., G.G.Z., and Y.S.P. contributed to drafting the text or preparing the figures.

Funding
This work was supported by National Natural Science Foundation of China (Grant No. 82030037 & No. 82201605); Beijing Natural Science Foundation (Grant No. L246017 & No. 7242070); the Translational and Application Project of Brain-inspired and Network Neuroscience on Brain Disorders, Beijing Municipal Health Commission (Grant No. 11000022T000000444685) and Fundamental Research Program of Shanxi Province (Grant No. 202203021222364).

Data availability
The datasets used and analyzed in the current study are available from the corresponding author on reasonable request.

Declarations

Ethics approval and consent to participate
All of the patient protocols, which were authorized by the Ethics Committee of Xuanwu Hospital, Capital Medical University, conformed to the ethical principles of the Declaration of Helsinki, and written informed consent was acquired from all of the human subjects (number: [2021]068).

Consent for publication
All presentations of case in our research have consent for publication.

Competing interests
The authors declare no competing interests.

Received: 18 August 2024 / Accepted: 24 November 2024
Published online: 30 November 2024

References

1. Ahring PK, Liao VWY, Gardella E, Johannesen KM, Krey I, Selmer KK et al (2022) Gain-of-function variants in GABRD reveal a novel pathway for neurodevelopmental disorders and epilepsy. Brain 145:1299–1309. https://doi.org/10.1093/brain/awab391
2. Alten B, Zhou Q, Shin OH, Esquivies L, Lin PY, White KI et al (2021) Role of aberrant spontaneous neurotransmission in SNAP25-Associated encephalopathies. Neuron 109:59–72e55. https://doi.org/10.1016/j.neuron.2020.10.012
3. Aroor A, Nguyen P, Li Y, Das R, Lugo JN, Brewster AL (2023) Assessment of tau phosphorylation and β-amyloid pathology in human drug-resistant epilepsy. Epilepsia Open 8:609–622. https://doi.org/10.1002/epi4.12744
4. Baldassari S, Ribierre T, Marsan E, Adle-Biassette H, Ferrand-Sorbets S, Bulteau C et al (2019) Dissecting the genetic basis of focal cortical dysplasia: a large cohort study. Acta Neuropathol 138:885–900. https://doi.org/10.1007/s00401-019-02061-5
5. Blauwblomme T, Dossi E, Pellegrino C, Goubert E, Iglesias BG, Sainte-Rose C et al (2019) Gamma-aminobutyric acidergic transmission underlies interictal epileptogenicity in pediatric focal cortical dysplasia. Ann Neurol 85:204–217. https://doi.org/10.1002/ana.25403
6. Blumcke I, Spreafico R, Haaker G, Coras R, Kobow K, Bien CG et al (2017) Histopathological findings in brain tissue obtained during Epilepsy surgery. N Engl J Med 377:1648–1656. https://doi.org/10.1056/NEJMoa1703784
7. Blumcke I, Budday S, Poduri A, Lal D, Kobow K, Baulac S (2021) Neocortical development and epilepsy: insights from focal cortical dysplasia and brain tumours. Lancet Neurol 20:943–955. https://doi.org/10.1016/s1474-4422(21)00265-9
8. Blumcke I, Cendes F, Miyata H, Thom M, Aronica E, Najm I (2021) Toward a refined genotype-phenotype classification scheme for the international consensus classification of focal cortical dysplasia. Brain Pathol 31:e12956. https://doi.org/10.1111/bpa.12956
9. Blümcke I, Thom M, Aronica E, Armstrong DD, Vinters HV, Palmini A et al (2011) The clinicopathologic spectrum of focal cortical dysplasias: a consensus classification proposed by an ad hoc Task Force of the ILAE Diagnostic Methods Commission. Epilepsia 52:158–174. https://doi.org/10.1111/j.1528-1167.2010.02777.x
10. Cepeda C, André VM, Hauptman JS, Yamazaki I, Huynh MN, Chang JW et al (2012) Enhanced GABAergic network and receptor function in pediatric cortical dysplasia type IIB compared with tuberous sclerosis complex. Neurobiol Dis 45:310–321. https://doi.org/10.1016/j.nbd.2011.08.015
11. Chen WT, Lu A, Craessaerts K, Pavie B, Sala Frigerio C, Corthout N et al (2020) Spatial Transcriptomics and In Situ Sequencing to Study Alzheimer's Disease. cell: 976–991 https://doi.org/10.1016/j.cell.2020.06.038
12. Chen F, Swartzlander DB, Ghosh A, Fryer JD, Wang B, Zheng H (2021) Clusterin secreted from astrocyte promotes excitatory synaptic transmission and ameliorates Alzheimer's disease neuropathology. Molecular neurodegeneration 16: 5 https://doi.org/10.1186/s13024-021-00426-7
13. Chen TS, Lai MC, Huang HI, Wu SN, Huang CW (2022) Immunity, Ion Channels and Epilepsy. Int J Mol Sci 23:6446. https://doi.org/10.3390/ijms23126446
14. Chen W, Zhang J, Zhang Y, Zhang J, Li W, Sha L et al (2023) Pharmacological modulation of autophagy for epilepsy therapy: opportunities and obstacles. Drug Discovery Today 28:103600. https://doi.org/10.1016/j.drudis.2023.103600
15. Crino PB (2011) mTOR: a pathogenic signaling pathway in developmental brain malformations. Trends Mol Med 17:734–742. https://doi.org/10.1016/j.molmed.2011.07.008
16. D'Antuono M, Louvel J, Köhling R, Mattia D, Bernasconi A, Olivier A et al (2004) GABAA receptor-dependent synchronization leads to ictogenesis in the human dysplastic cortex. Brain 127:1626–1640. https://doi.org/10.1093/brain/awh181
17. D'Gama AM, Woodworth MB, Hossain AA, Bizzotto S, Hatem NE, LaCoursiere CM et al (2017) Somatic mutations activating the mTOR pathway in dorsal telencephalic progenitors cause a continuum of cortical dysplasias. Cell Rep 21:3754–3766. https://doi.org/10.1016/j.celrep.2017.11.106
18. De Miguel Z, Khoury N, Betley MJ, Lehallier B, Willoughby D, Olsson N et al (2021) Exercise plasma boosts memory and dampens brain inflammation via clusterin. Nature 600:494–499. https://doi.org/10.1038/s41586-021-04183-x
19. Herold C, Bidmon HJ, Pannek HW, Hans V, Gorji A, Speckmann EJ et al (2018) ATPase N-ethylmaleimide-sensitive Fusion protein: a Novel Key Player for causing spontaneous network excitation in human temporal lobe Epilepsy. Neuroscience 371:371–383. https://doi.org/10.1016/j.neuroscience.2017.12.013

20. Heyne HO, Artomov M, Battke F, Bianchini C, Smith DR, Liebmann N et al (2019) Targeted gene sequencing in 6994 individuals with neurodevelopmental disorder with epilepsy. Genet Medicine: Official J Am Coll Med Genet 21:2496–2503. https://doi.org/10.1038/s41436-019-0531-0
21. Hwang B, Lee JH, Bang D (2018) Single-cell RNA sequencing technologies and bioinformatics pipelines. Exp Mol Med 50:1–14. https://doi.org/10.1038/s12276-018-0071-8
22. Joglekar A, Prjibelski A, Mahfouz A, Collier P, Lin S, Schlusche AK et al (2021) A spatially resolved brain region- and cell type-specific isoform atlas of the postnatal mouse brain. Nat Commun 12:463. https://doi.org/10.1038/s41467-020-20343-5
23. Kim JH, Park JH, Lee J, Park JW, Kim HJ, Chang WS et al (2023) Ultra-low Level somatic mutations and structural variations in focal cortical dysplasia type II. Ann Neurol 93:1082–1093. https://doi.org/10.1002/ana.26609
24. Kumar R, Jangir DK, Verma G, Shekhar S, Hanpude P, Kumar S et al (2017) S-nitrosylation of UCHL1 induces its structural instability and promotes α-synuclein aggregation. Sci Rep 7:44558. https://doi.org/10.1038/srep44558
25. Lee WS, Baldassari S, Stephenson SEM, Lockhart PJ, Baulac S, Leventer RJ (2022) Cortical dysplasia and the mTOR pathway: how the study of human brain tissue has led to insights into Epileptogenesis. Int J Mol Sci 23. https://doi.org/10.3390/ijms23031344
26. Li YF, Scerif F, Picker SR, Stone TJ, Pickles JC, Moulding DA et al (2021) Identifying cellular signalling molecules in developmental disorders of the brain: evidence from focal cortical dysplasia and tuberous sclerosis. Neuropathol Appl Neurobiol 47:781–795. https://doi.org/10.1111/nan.12715
27. Lim JS, Gopalappa R, Kim SH, Ramakrishna S, Lee M, Kim WI et al (2017) Somatic mutations in TSC1 and TSC2 cause focal cortical dysplasia. Am J Hum Genet 100:454–472. https://doi.org/10.1016/j.ajhg.2017.01.030
28. Liu R, Xing Y, Zhang H, Wang J, Lai H, Cheng L et al (2022) Imbalance between the function of na(+)-K(+)-2Cl and K(+)-Cl impairs Cl(-) homeostasis in human focal cortical dysplasia. Front Mol Neurosci 15:954167. https://doi.org/10.3389/fnmol.2022.954167
29. Maniatis S, Äijö T, Vickovic S, Braine C, Kang K, Mollbrink A et al (2019) Spatiotemporal dynamics of molecular pathology in amyotrophic lateral sclerosis. Science 364:89–93. https://doi.org/10.1126/science.aav9776
30. Mi Z, Graham SH (2023) Role of UCHL1 in the pathogenesis of neurodegenerative diseases and brain injury. Ageing Res Rev 86:101856. https://doi.org/10.1016/j.arr.2023.101856
31. Mizushima N, Levine B (2020) Autophagy in Human diseases. N Engl J Med 383:1564–1576. https://doi.org/10.1056/NEJMra2022774
32. Mondello S, Palmio J, Streeter J, Hayes RL, Peltola J, Jeromin A (2012) Ubiquitin carboxy-terminal hydrolase L1 (UCH-L1) is increased in cerebrospinal fluid and plasma of patients after epileptic seizure. BMC Neurol 12:85. https://doi.org/10.1186/1471-2377-12-85
33. Munson MJ, Ganley IG (2015) MTOR, PIK3C3, and autophagy: signaling the beginning from the end. Autophagy 11:2375–2376. https://doi.org/10.1080/15548627.2015.1106668
34. Najm I, Lal D, Alonso Vanegas M, Cendes F, Lopes-Cendes I, Palmini A et al (2022) The ILAE consensus classification of focal cortical dysplasia: an update proposed by an ad hoc task force of the ILAE diagnostic methods commission. Epilepsia 63:1899–1919. https://doi.org/10.1111/epi.17301
35. Nakashima M, Saitsu H, Takei N, Tohyama J, Kato M, Kitaura H et al (2015) Somatic mutations in the MTOR gene cause focal cortical dysplasia type IIb. Ann Neurol 78:375–386. https://doi.org/10.1002/ana.24444
36. Navarro JF, Croteau DL, Jurek A, Andrusivova Z, Yang B, Wang Y et al (2020) Spatial Transcriptomics reveals genes Associated with Dysregulated mitochondrial functions and stress signaling in Alzheimer Disease. iScience 23:101556. https://doi.org/10.1016/j.isci.2020.101556
37. Ortiz C, Navarro JF, Jurek A, Märtin A, Lundeberg J, Meletis K (2020) Molecular atlas of the adult mouse brain. Sci Adv 6:eabb3446. https://doi.org/10.1126/sciadv.abb3446
38. Pohl C, Dikic I (2019) Cellular quality control by the ubiquitin-proteasome system and autophagy. Science 366:818–822. https://doi.org/10.1126/science.aax3769
39. Poliquin S, Kang JQ (2022) Disruption of the ubiquitin-proteasome system and elevated endoplasmic reticulum stress in Epilepsy. Biomedicines 10:647. https://doi.org/10.3390/biomedicines10030647
40. Rana A, Musto AE (2018) The role of inflammation in the development of epilepsy. J Neuroinflammation 15:144. https://doi.org/10.1186/s12974-018-1192-7
41. Sim NS, Ko A, Kim WK, Kim SH, Kim JS, Shim KW et al (2019) Precise detection of low-level somatic mutation in resected epilepsy brain tissue. Acta Neuropathol 138:901–912. https://doi.org/10.1007/s00401-019-02052-6
42. Ståhl PL, Salmén F, Vickovic S, Lundmark A, Navarro JF, Magnusson J et al (2016) Visualization and analysis of gene expression in tissue sections by spatial transcriptomics. Science 353:78–82. https://doi.org/10.1126/science.aaf2403
43. Stuart T, Butler A, Hoffman P, Hafemeister C, Papalexi E, Mauck WM 3rd, et al (2019) Comprehensive Integration of Single-Cell Data. Cell 177:1888–1902e1821. https://doi.org/10.1016/j.cell.2019.05.031
44. Tarkowski B, Kuchcinska K, Blazejczyk M, Jaworski J (2019) Pathological mTOR mutations impact cortical development. Hum Mol Genet 28:2107–2119. https://doi.org/10.1093/hmg/ddz042
45. Vezzani A, Fujinami RS, White HS, Preux PM, Blümcke I, Sander JW et al (2016) Infections, inflammation and epilepsy. Acta Neuropathol 131:211–234. https://doi.org/10.1007/s00401-015-1481-5
46. Wang Y, Wang L, Blümcke I, Zhang W, Fu Y, Shan Y et al (2022) Integrated genotype-phenotype analysis of long-term epilepsy-associated ganglioglioma. Brain Pathol 32:e13011. https://doi.org/10.1111/bpa.13011
47. Wang Y, Yu T, Blümcke I, Cai Y, Sun K, Gao R et al (2023) The clinico-pathological characterisation of focal cortical dysplasia type IIb genetically defined by MTOR mosaicism. Neuropathol Appl Neurobiol 49:e12874. https://doi.org/10.1111/nan.12874
48. Willis EF, MacDonald KPA, Nguyen QH, Garrido AL, Gillespie ER, Harley SBR et al (2020) Repopulating Microglia promote Brain Repair in an IL-6-Dependent manner. Cell 180:833–846e816. https://doi.org/10.1016/j.cell.2020.02.013
49. Wojtas AM, Sens JP, Kang SS, Baker KE, Berry TJ, Kurti A et al (2020) Astrocyte-derived clusterin suppresses amyloid formation in vivo. Mol Neurodegeneration 15:71. https://doi.org/10.1186/s13024-020-00416-1
50. Yi Z, Song Z, Xue J, Yang C, Li F, Pan H et al (2022) A heterozygous missense variant in the YWHAG gene causing developmental and epileptic encephalopathy 56 in a Chinese family. BMC Med Genom 15:216. https://doi.org/10.1186/s12920-022-01377-8
51. Zhang M, Cai F, Zhang S, Zhang S, Song W (2014) Overexpression of ubiquitin carboxyl-terminal hydrolase L1 (UCHL1) delays Alzheimer's progression in vivo. Sci Rep 4:7298. https://doi.org/10.1038/srep07298
52. Zhang Z, Liu Q, Liu M, Wang H, Dong Y, Ji T et al (2018) Upregulation of HMGB1-TLR4 inflammatory pathway in focal cortical dysplasia type II. J Neuroinflammation 15:27. https://doi.org/10.1186/s12974-018-1078-8
53. Zhong S, Zhao Z, Xie W, Cai Y, Zhang Y, Ding J et al (2021) GABAergic Interneuron and neurotransmission are mTOR-Dependently disturbed in experimental focal cortical dysplasia. Mol Neurobiol 58:156–169. https://doi.org/10.1007/s12035-020-02086-y
54. Zimmer TS, Broekaart DWM, Luinenburg M, Mijnsbergen C, Anink JJ, Sim NS et al (2021) Balloon cells promote immune system activation in focal cortical dysplasia type 2b. Neuropathol Appl Neurobiol 47:826–839. https://doi.org/10.1111/nan.12736

Publisher's note